# A survey of 71 earthquake bursts across southern California: Exploring the role of pore fluid pressure fluctuations and aseismic slip as drivers

John E. Vidale[1] and Peter M. Shearer[2]

Received 8 September 2005; revised 3 January 2006; accepted 2 February 2006; published 25 May 2006.

[1] We investigate the cause of seismicity bursts by examining a waveform-relocated catalog for southern California between 1984 and 2002 and systematically identifying 71 isolated sequences of 40 or more earthquakes occurring within a 2-km-radius volume and a 4-week interval. Fifty-seven of the 71 bursts are difficult to interpret as primarily a main shock and its Omori-law-abiding foreshocks and aftershocks because they exhibit a more complicated evolution in space, time, and magnitude; we identify 18 of these sequences as particularly swarm-like. Evidence against a simple cascade of elastic stress triggering includes the presence of an interval of steady seismicity rate, the tendency of the largest event to strike later in the sequence, the large spatial extent of some of the swarms compared to their cumulative moment, and the weak correlation between the number of events in each burst and the magnitude of the largest event in each burst. Shallow sequences and normal faulting mechanism sequences are most likely to be swarm-like. The tendencies of the hypocenters in the swarm-like sequences to occur on vertical planes and expand over time suggest pore fluid pressure fluctuations as the most likely mechanism driving the swarm-like seismicity bursts. However, episodic aseismic slip could also be at least partly responsible and might provide a more compelling explanation for the steady rate of seismicity during swarms, whereas fluid pressure perturbations might be expected to diminish more rapidly with time. Both aftershock-like and swarm-like seismicity bursts are distributed across the entire study region, indicating that they are a general feature of tectonic faulting, rather than limited to a few geological conditions such as volcanic or geothermal areas.

**Citation:** Vidale, J. E., and P. M. Shearer (2006), A survey of 71 earthquake bursts across southern California: Exploring the role of pore fluid pressure fluctuations and aseismic slip as drivers, *J. Geophys. Res.*, *111*, B05312, doi:10.1029/2005JB004034.

## 1. Introduction

[2] Earthquake bursts, broadly defined as many earthquakes striking in limited space and time, are generally attributed either to a cascade of elastic fault rupture or to the hidden influence of fluids or aseismic slip, particularly in volcanic areas and on transform faults. Such bursts have been recognized and studied for nearly as long as there have been seismic networks. Many such bursts are understood as aftershocks initially delineating the rupture planes of large earthquakes [*Scholz*, 1990], and often expanding slightly later [*Henry and Das*, 2001; *Tajima and Kanamori*, 1985a, 1985b]. However, other bursts have no main shock of sufficient magnitude to explain the extent of the hypocentral distribution [*Mogi*, 1963], and are commonly termed swarms. Some swarms have a time evolution of hypocenters that indicates the presence of aseismic processes.

[3] Seismicity bursts are common in many tectonic settings. Volcanic regions are particularly prone to seismicity bursts of several types, which have been tied with more or less direct evidence to magmatic processes [*Dzurisin*, 2003]. A global compilation of 385 volcanic swarms, which tend to be shallower than tectonic swarms, found a median duration of five days, with longer durations correlating with swarms that preceded eruptions [*Benoit and McNutt*, 1996].

[4] Seismicity near the Long Valley caldera in California has been a fruitful target for study. The observation of nondouble-couple source mechanisms for large earthquakes at the time of swarms [*Dreger et al.*, 2000] supports various magma-related scenarios for episodicity and time migration of those swarms. More directly, upward and sideways migration rates ranging from 30 m/day to 0.5 km/hr, possibly due to intrusion and overpressure of rising and spreading magmatic fluid, have been noted [*Hill et al.*, 1990; *Hough et al.*, 2000; *Prejean et al.*, 2003].

[5] One particularly well studied swarm region is near Bohemia in Europe [*Hainzl*, 2004; *Hainzl and Fischer*, 2002; *Hainzl and Ogata*, 2005; *Hainzl et al.*, 2003]. An

[1]Institute of Geophysics and Planetary Physics, University of California, Los Angeles, California, USA.

[2]Scripps Institution of Oceanography, Institute of Geophysics and Planetary Physics, University of California, San Diego, La Jolla, California, USA.


0148-0227/06/2005JB004034$09.00

initial stage with somewhat spatially and temporally independent seismicity is evidence for underlying fluid movement triggering the swarm, interpreted as degassing of an active magma body in the upper mantle [*Bräuer et al.*, 2003], and tensile components of faulting have been inferred, consistent with fluid pressurization driving crack opening during earthquakes [*Horálek et al.*, 2002]. Progressive rupture in Bohemian swarms is indicated by frequent observations of earthquakes closely following previous events in space and time [*Fischer and Horálek*, 2005].

[6] Seismicity bursts on ridge transform faults also tend to occur in swarms. Compared to earthquake sequences in continental regions, ridge transform swarms have far higher rates of foreshocks and lower rates of aftershocks [*McGuire et al.*, 2005]. Slip on these faults has been argued to predominantly occur aseismically [*Bird and Kagan*, 2004; *Boettcher and Jordan*, 2004], and seismicity has been inferred to accompany times of accelerated aseismic slip [*McGuire et al.*, 2005].

[7] In this paper, we take advantage of recent dramatic improvements in earthquake relocation accuracy allowed by waveform cross correlation [*Shearer et al.*, 2005] in order to systematically examine the behavior of seismicity bursts in southern California. We find a range of patterns with some similarity to ridge-transform and volcanic swarms across much of our study area, and we explore the underlying reasons why bursts occur.

## 2. Selection of Earthquake Bursts

[8] Our selection process is intended to identify only the cleanest of the seismicity bursts. We select isolated compact pockets of intense seismicity that start relatively abruptly in a sufficient quantity for a fruitful interrogation. The motivation for our criteria is to avoid protracted and widespread aftershock sequences of large events and persistent nests of seismicity with extended and complex geometries, in which earthquake interaction is likely to be more difficult to unravel.

[9] Delineation of the geometry and time evolution of seismicity benefits from location accuracy, so we use the SHLK_1.01 catalog, which provides cross-correlation relocations for southern California for the years 1984 to 2002 [*Shearer et al.*, 2005]. We consider only latitudes from 33° to 36°N and longitudes from 116 to 119°W to assure a good geometry of network seismometer sites for relocations. Estimated relative location errors are generally less than 100 m and often less than 20 m within individual similar-event clusters.

[10] A complication is that the SHLK_1.01 locations are most accurate only for events within similar-waveform event clusters. Relative location accuracy between events in different clusters is much worse. Thus we consider only the pattern of locations within individual similar-event clusters in examining the shape and time evolution of the seismicity geometry.

[11] Our selection criteria had three requirements, designed to identify compact and isolated bursts of seismicity. (1) An initial event must be followed by at least 39 events within a radius of 2 km in 28 days, (2) there must be three or fewer events in the prior 28 days within the same 2 km radius, and (3) no more than 20% more events occur between 2 and 4 km from the initiating event in the same 28 days afterward. We simply test each of the 166,525 events in SHLK_1.01 that are relocated with waveform correlation in our study area as a potential initial event.

[12] Next, we visually examine the three-dimensional (3-D) distribution of seismicity in each burst with two different selection criteria including (1) earthquakes located solely by traveltimes as well as earthquakes located by waveform cross correlation and (2) waveform-correlated seismicity only from a single cluster. We analyze the spatiotemporal evolution of the seismicity only with the second, most restrictive group, which has by far the best relative location accuracy.

[13] A few details warrant additional comment. Three sequences had as many as four foreshocks after manual adjustment of the initiating event. The biggest events in a sequence sometimes are not in the dominant cross-correlation event cluster because larger earthquakes have additional waveform complexity resulting from their extended rupture areas and durations compared to the smaller earthquakes, which are effectively point sources in space and time. In such occasional omissions of the main shock hypocenter from the dominant cluster, we will implicitly assume that the poorly located larger events fall on the trend of the seismicity within the cluster. However, when precise location is not necessary, as in specifying the largest event in a burst, we consider all events in the 28 days of the burst, whether waveform correlated or not. We rejected five seismicity bursts composed of components from several distinct clusters, but retain those bursts for which a few earthquakes in secondary clusters are present but are only minor constituents of the seismicity.

[14] Because of our selection criteria, all of our chosen sequences start abruptly at the beginning of our 4-week window. In most cases, activity ceases or diminishes to a low rate after 28 days. However, for a few sequences the seismicity continues at a relatively steady rate for several months. There is nonetheless an initial concentration of activity near the beginning of these sequences and for simplicity we assume a fixed 28-day selection window for all of our analyses.

[15] We identify 71 sequences, which span most of our study region (Figure 1). Fourteen clusters begin with their largest events (we include one cluster that started with a foreshock just 15 s before the main shock) and resemble main shock/aftershock sequences; these are marked with crosses in Figure 1. We note that the Oak Ridge sequence, which was identified by one of us in a previous paper [*Shearer*, 1998], is included, but just barely, with 41 earthquakes, one more than the minimum total number of events necessary for selection. Most other clusters identified in previous analyses of similar event groups in aftershock sequences [*Astiz and Shearer*, 2000; *Astiz et al.*, 2000; *Shearer*, 1997; *Shearer et al.*, 2003] and along the Imperial Fault [*Shearer*, 2002] are not included because they are too protracted in time.

[16] The depth distribution of our selected clusters is not strikingly different than that of the overall seismicity (Figure 2). All the sequences are well above the lower depth limits of seismicity in their region [*Magistrale*, 2002]. A smaller proportion of the clusters tend to be shallower than 4 km or deeper than 10 km depth than in the background seismicity. An underpopulation of aftershock sequences for

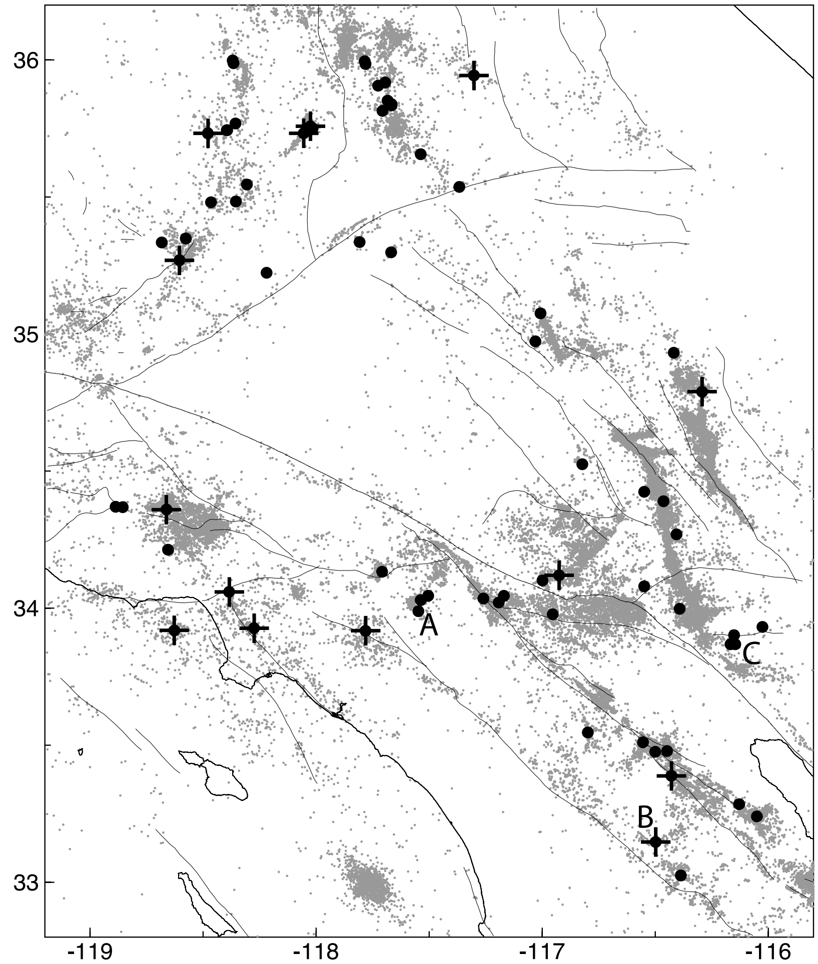


**Figure 1.** Locations of the 71 earthquake clusters in southern California (black dots), together with 1984 to 2002 seismicity from the SHLK_1.01 catalog (gray dots) and active Quaternary faults (thin lines). The clusters marked with the crosses began with their largest event and so resemble main shocks with aftershocks. The clusters labeled A, B, and C are presented in Figures 3, 4, and 5.

deep events compared to shallow events has often been observed, and may help explain the paucity in our data set of seismicity bursts below 10 km depth. The areal distribution of our clusters is similar to that of the entire seismicity catalog in being spread across the San Andreas Fault segments, the Transverse Ranges, and the Mojave (Figure 1).

## 3. Three Case Studies

[17] Many of the clusters have interesting temporal and spatial patterns. We begin by showing three examples, before examining the features more quantitatively to find general cluster properties.

[18] Figure 3 shows a swarm of 230 events that began on 15 July 1994, between Pomona and Riverside. The seismicity is aligned into a plane and the face-on view is shown. The maximum magnitude event ($M$ 3.4) occurs during the middle of the sequence. We will use the term ‘‘swarm-like’’ to describe clusters of this type, which do not have a clear main shock/aftershock pattern. The spatial extent of the sequence gradually grows during the 28 days, from an initial region less than a kilometer across to the full 2.5 km length of the plane. This example is typical of the

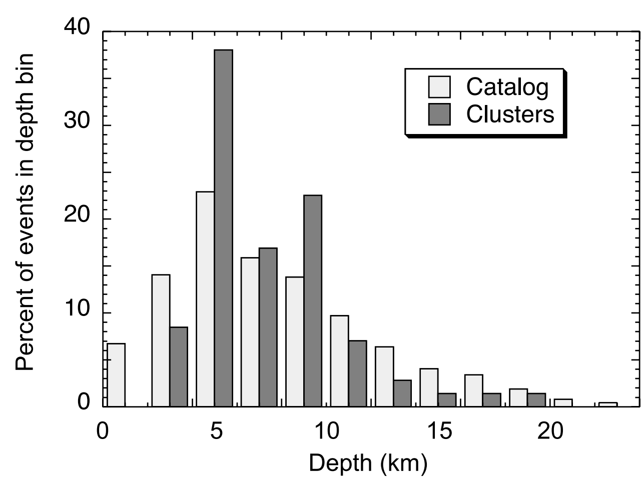


**Figure 2.** Comparison of the depth distribution of the clusters (dark gray) with that of the background seismicity (light gray).

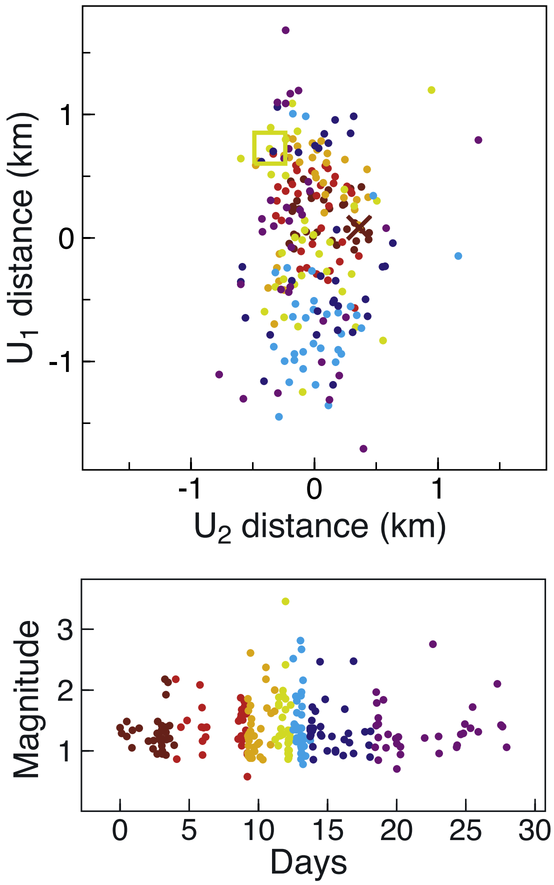


**Figure 3.** A swarm-like cluster of 230 earthquakes at 5 km depth near Ontario, California, beginning on 15 July 1994 (see A label in Figure 1). (top) Events projected onto the best fitting plane (details of this projection are explained in the principal component analysis section), with the sequence divided into seven time groups by color with equal numbers of events in each group. The divisions between colors occur at 3.9, 9.2, 11.2, 12.5, 13.7, and 18.1 days. The first event is indicated with a cross; the largest event is shown with a square. (bottom) Catalog magnitude versus time from the first event. Events with no magnitude are assigned $M = 0.9$, and a random number between $-0.05$ and 0.05 is added to the magnitudes for plotting purposes.

swarm-like clusters; most exhibit at least some spatially coherent time evolution, which often takes the form of spreading outward or moving laterally from an initiation point. The details of these temporal trends can be complex, however, and not all of the clusters align clearly into planar features.

[19] Figure 4 shows a cluster of 190 events that began with a $M$ 4.5 main shock on 10 October 1984. We will use the term “aftershock-like” to describe clusters of this type, where the largest earthquake occurs at the beginning of the sequence and subsequent events are smaller. The seismicity for this example forms a complicated 3-D pattern and does not align into a single well-defined plane. There is little temporal evolution in the spatial pattern; most parts of the spatial distribution have events occurring throughout the sequence. This behavior is typical of most of the aftershock-like clusters, in which the aftershock region seems to “light up” immediately following the main shock and exhibits relatively little spreading with time.

[20] However, these differences between the behavior of the swarm-like and aftershock-like clusters are not always so clear. Figure 5 shows a group of 189 earthquakes that began on 7 April 1990. As in the example of Figure 4, the seismicity forms a complicated 3-D pattern. It appears swarm-like because it has no well-defined main shock. However, it has only a weak suggestion of temporal evolution in that the events within the first few days span almost the entire length of the cluster. As we will show in more detail later, the swarm-like clusters vary in the tendency for their seismicity to spread and evolve. In contrast, the aftershock-like clusters almost always show little spreading and migration.

[21] We divided the 71 sequences into three groups; 14 “aftershock-like” sequences, (defined by having their largest event first, or 15 s later in one case), 18 “swarm-like” sequences (defined by having the most voluminous bursts for their cumulative moment, having their largest event late

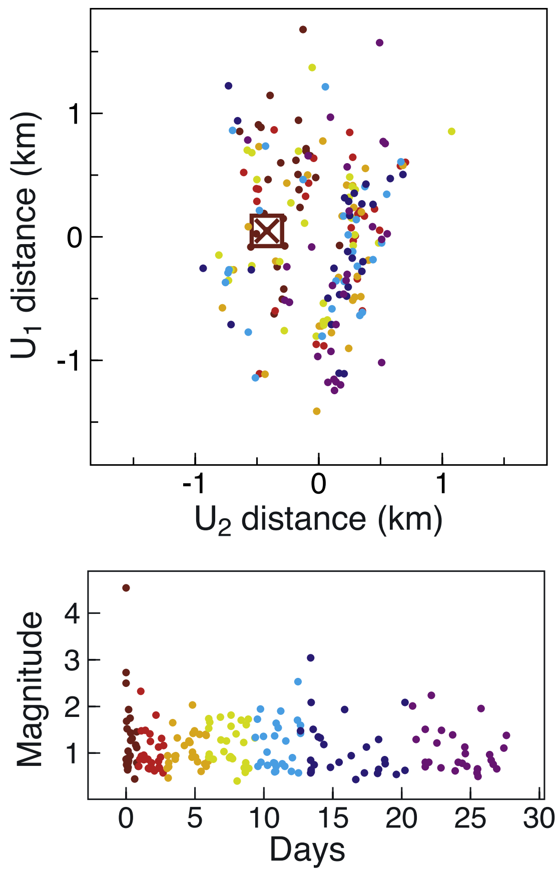


**Figure 4.** An aftershock-like cluster of 190 earthquakes at 9 km depth near Grapevine Mountain, California, beginning on 10 October 1984 (see B label in Figure 1). (top) Events projected onto the best fitting plane, with the sequence divided into seven time groups by color with equal numbers of events in each group. The divisions between colors occur at 0.9, 2.7, 6.0, 9.4, 12.7, and 20.2 days. The first and largest event is indicated with a cross; the largest event is shown with a square. (bottom) Catalog magnitude versus time from the first event. Events with no magnitude are assigned $M = 0.9$, and a random number between $-0.05$ and 0.05 is added to the magnitudes for plotting purposes.

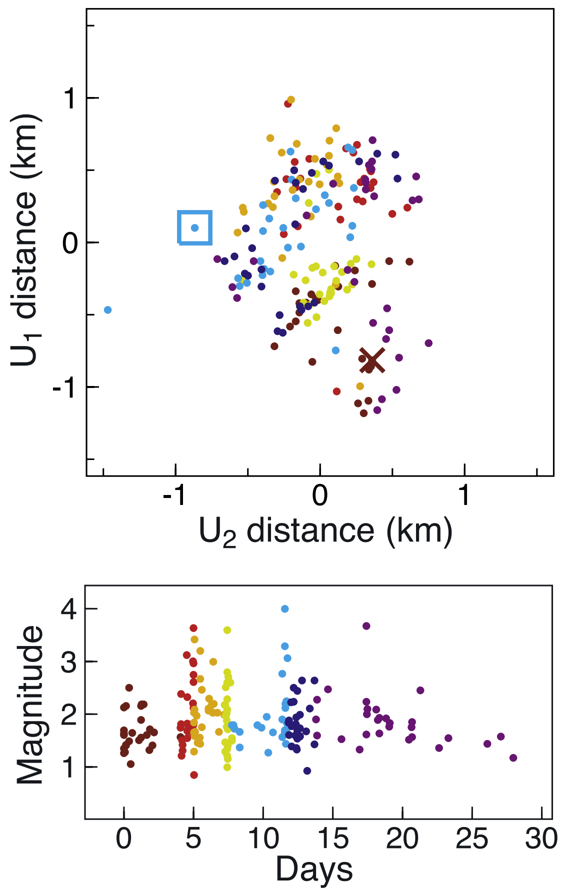


**Figure 5.** A swarm-like cluster of 189 earthquakes at 3-km depth near Pushawalla Canyon, California, beginning on 7 April 1990 (see C label in Figure 1). (top) Events projected onto the best fitting plane, with the sequence divided into seven time groups by color with equal numbers of events in each group. The divisions between colors occur at 4.1, 5.0, 7.2, 7.8, 11.7, and 13.4 days. The first event is indicated with a cross; the largest event is shown with a square. (bottom) Catalog magnitude versus time from the first event. Events with no magnitude are assigned $M = 0.9$, and a random number between $-0.05$ and 0.05 is added to the magnitudes for plotting purposes.

in the sequence, having the most expansion over time, and having a relatively large number of events with respect to the largest magnitude), and the 39 "average" sequences in between. We show plots of these and other burst measures below.

## 4. Spatial Extent and Earthquake Count of Seismicity Bursts

[22] The large radius of these clusters compared to the magnitudes of the largest events, shown in Figure 6, is evidence that many of the bursts differ from a simple model of a main shock with aftershocks along its rupture plane. Sequences whose largest magnitude event is larger tend to be more spatially extensive, as would be expected for main shock–aftershock sequences. However, the trend is far weaker than would be predicted by a constant stress drop scaling, which is shown by the lines on Figure 6. In addition, many "main shocks" strike later in the sequence after the seismicity volume has already been filled by smaller-magnitude activity.

[23] Very low stress drops would be necessary to distribute the rupture in the largest events across the entire region for some of the seismicity bursts. The stress drops have been estimated in most of the *M* 2 to 3.5 events in 43 out of 71 of these bursts [*Shearer et al.*, 2006]. The median stress drop in these bursts ranges from 0.3 to 18 MPa, with a median value of 1.6 MPA. These values are comparable in size and variability to other small earthquakes in southern California. However, the study is limited to earthquakes below $M \sim 3.4$ because records from larger events are clipped. Precise comparisons between earthquake source sizes and burst dimensions are difficult because of the modeling assumptions necessary to estimate source radius from corner frequency measurements and the uncertainties in quantifying burst radius (here defined as the average distance to the swarm centroid). We note, however, that no correlation appears between the stress drops estimated from the seismic waves and the ratio of moment divided by the radius of the sequence cubed, as would have been observed if the entire seismicity area ruptured seismically during the sequence.

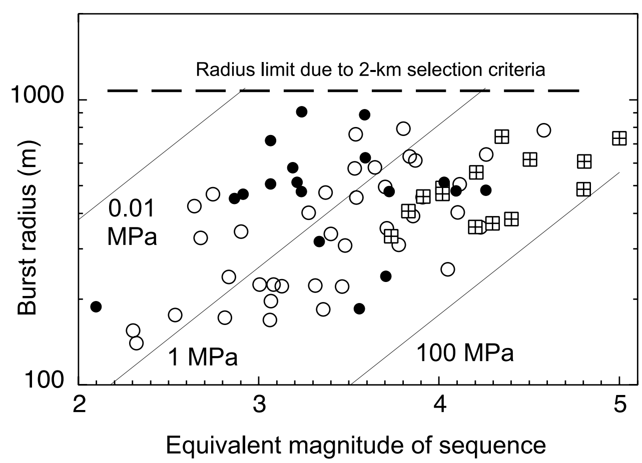


**Figure 6.** Estimated burst radius compared to the equivalent magnitude of the 71 seismicity sequences. The radius is the mean of the distances to the events in each sequence from the centroid of the events. Lines show the radii of circular faulting for stress drops of 0.01, 1.0, and 100 MPa as a function of magnitude [*Lay and Wallace*, 1995]. A limitation of this plot is that our selection process, which chooses only seismicity bursts contained mostly within a 2-km-radius sphere, results in about a 1-km upper bound on burst dimension. The 14 bursts in which the largest event is the initiating event are marked by crossed squares, the 18 most swarm-like are marked by solid circles, and the rest are marked by open circles. The equivalent magnitude is the magnitude of the sum of the moments of the events in a sequence. We estimate moment using the definition of $M_w$ [*Kanamori*, 1977], assuming that the local magnitudes are approximately equal to the moment magnitudes.

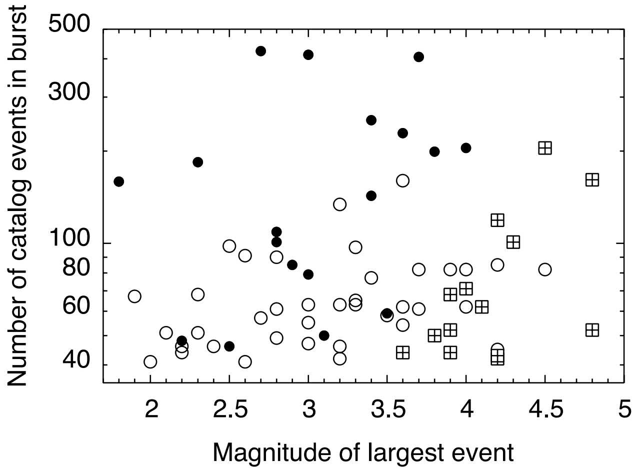


**Figure 7.** A comparison between the total number of events and the magnitude of the largest event in the 71 seismicity bursts. There is no tendency for larger main shocks to generate sequences with more events. Symbols are defined as in Figure 6.

[24] At least a third of the bursts are too large to plausibly match the rupture area of their largest event. The events on the right side of the plot tend to be similar to traditional main shock–aftershock sequences in that the 14 sequences that have their largest event at the start of the sequence (crossed squares in Figure 6) are all in that region.

[25] Figure 7 shows additional evidence that the swarm-like bursts are not driven by their biggest event: the observation that the number of earthquakes captured by the network is largely uncorrelated with the size of the largest event.

[26] Bigger "main shocks" might be expected to both light up larger volumes in Figure 6 and give rise to more aftershocks in Figure 7. Their failure to show this result suggests that the more swarm-like sequences are a response to an underlying geophysical impetus rather than simply a cascade of ruptures embedded in an elastic medium.

[27] Figures 6 and 7 show that swarm-like sequences probably have higher $b$ values than aftershock-like sequences. We do not compute $b$ values directly because most of the events in our sequences are at or below the completeness threshold magnitude for the catalog. One could interpret the larger volumes of the swarm-like sequences to arise from lower stress drops, which are frequently associated with regions of higher $b$ value, however this argument is not supported by stress drop measurements [*Shearer et al.*, 2006], which indicate that the seismic stress drops do not differ significantly among our three sequence categories.

[28] A potential concern with our approach is the inclusion of many events below the completeness level of our catalog, which is roughly M2. A lower completeness level near some cluster locations compared to other locations could result in some apparently "swarmy" sequences at the former, and other more main shock-like sequences at the latter, mimicking the pattern shown in Figure 7, although our other findings are unlikely to be affected. We examined this issue in some detail, and found that the bulk of our catalog is between M1 and M2, so little data would remain were we to solely analyze data in a complete catalog. However, there is no apparent correlation between the locations of the swarmy clusters and areas of poor network coverage, and the greater numbers of events in swarmy sequences is well explained if the average $b$ value of the swarmy earthquake clusters is about 0.3 higher than the other two styles. Given the many uncertainties in measuring $b$ values for small, selected, and incomplete catalogs, further analysis is not warranted in this paper.

## 5. Temporal Evolution of Earthquake Clusters

[29] The durations of the seismicity bursts, measured as the median time from initiation, range from 0.22 days to the limit possible in the 28-day window examined. The median and mean event time lags from the first event time is 4.5 and 6.2 days, comparable to the typical duration found for volcanic swarms [*Benoit and McNutt*, 1996]. The seismicity rate in the month preceding the bursts is low and, on average, fairly steady. In addition, a few of the events in the preceding month are true foreshocks, generally less than a day before the picked start of the burst, as is typically observed for foreshocks in general [*Jones and Molnar*, 1979]. The average rate of activity in the month after initiation is about 100 times greater than in the month before.

[30] The average activity rate of the 71 bursts diminishes with the passage of time after initiation. The observed seismicity falloff rate, if the bursts are combined without renormalizing the timescale (as we will do next), is similar, for example, to that found in our study of a comparable data set of moderate earthquakes and their aftershocks in Japan, in which activity diminishes as $t^{-p}$, where $t$ is time; $p$ in that study is roughly in the range 0.7 to 0.9, depending on the criteria for selecting main shocks, across the time range from tens of seconds to years [*Omori*, 1895; Z. Peng et al., Anomalous seismicity rate immediately before and after main shock rupture from high-frequency waveforms, in Japan, submitted to *Journal of Geophysical Research*, 2006].

[31] We can obtain a better measure of the time evolution among the bursts by first renormalizing to equalize all swarm durations before summing all the bursts. We define the average duration of each sequence to be the mean of the time lags of the events after the time of burst initiation, as illustrated in Figure 8.

[32] Only the 57 out of 71 bursts that do not start with their largest event, i.e., the swarm-like and average sequences, are included to capture the "swarmy" aspect of the sequences most clearly, and the event timing is compared with several Omori-style curves in Figure 9. The two salient features of Figure 9a are the initial peak, with about 10% of the events, and the roughly steady rate that lasts until after the mean time lag in the sequences. The initial peak is likely composed of aftershocks of the initiating earthquake, which is sometimes one of the larger events in the sequence, or the largest event, which disproportionately strikes early, even though we have excluded swarms in which it occurs first. Following the initial peak, the seismicity rate is steady through most of the burst. Then the rate diminishes rapidly after about 1.5 times the mean delay.

[33] Figure 9b shows that the largest events in each sequence follow a similar pattern, although the small sample size of the data set limits resolution. As opposed to normal

main shock–aftershock patterns, in which the largest events are generally first, in these sequences, the largest events appear throughout the sequence in a similar proportion to the smaller events.

[34] We infer that the average profile shown in Figure 9 is a mix of components of two end-members: (1) a normal main shock–aftershock Omori law and (2) swarm-like behavior with an emergent beginning leading to periods of steady seismicity, without an initial peak.

## 6. Spatiotemporal Evolution and Other Systematics of Earthquake Clusters

[35] In space, the seismicity bursts tend to expand away from their point of initiation (Figure 10). The aftershock-

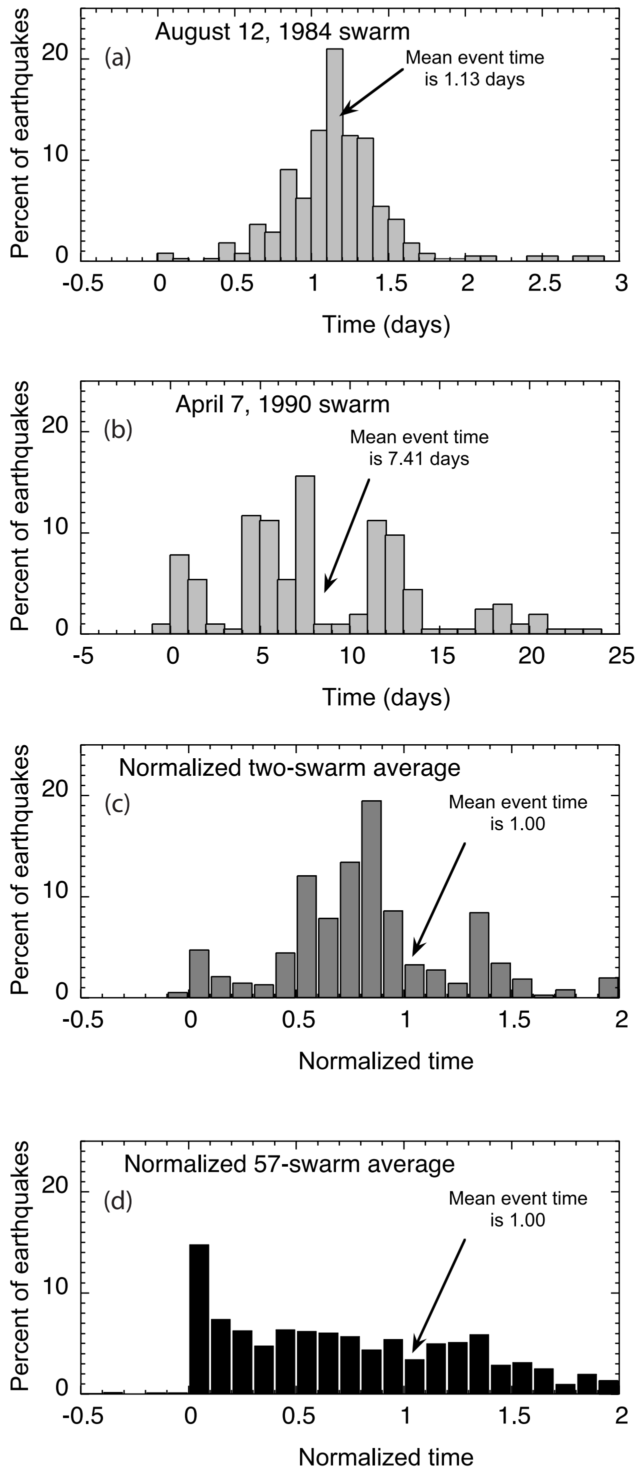


**Figure 8.** Method and examples of time normalization. (a) Number of events as a function of time relative to initiation for one burst. (b) The same for a second burst. (c) The result of rescaling the time so that each burst starts at time 0 and has a mean time of 1, then averaging the two bursts. (d) Result of rescaling time and summing the 57 sequences that do not start with their largest event.

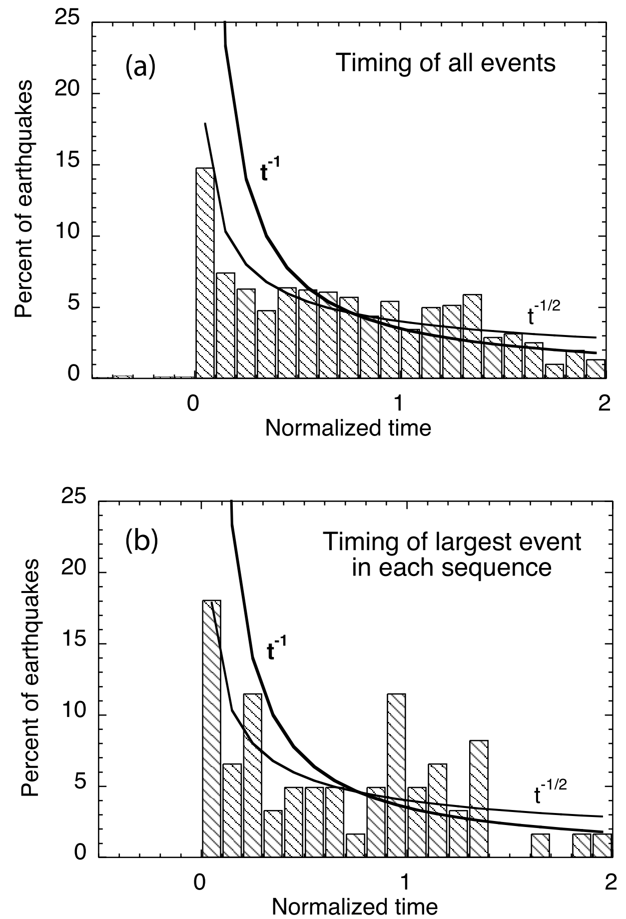


**Figure 9.** Rate of seismicity as a function of time after burst initiation divided by the mean time over the entire burst since initiation. The 57 bursts that do not start with their largest event are plotted. (a) All the events in the 57 sequences. (b) The largest event in the 57 sequences. Seven bursts appear twice in Figure 9b because their two largest events have the same magnitude. Although the median would have provided a more robust measure by preventing late events from contributing disproportionately to the mean time for short seismicity bursts, unfortunately, it also generates an artificial peak in seismicity rate at the time of the median because near the median time, there is a concentration of events more often than random.

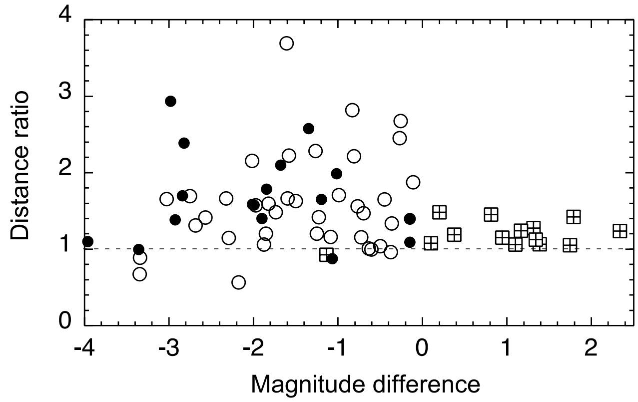


**Figure 10.** Temporal expansion of the sequences versus the relative magnitude of their first event. The expansion is measured as the distance ratio (*y* axis), defined as the ratio of the median distance from the initiating event between the second and first halves of the seismicity. This parameter is near unity for sequences with little or no spatial expansion. The magnitude difference (*x* axis) is the difference in magnitude between the first event and the largest remaining event. The 14 sequences that begin with their largest events have positive magnitude differences and plot to the right. These aftershock-like sequences clearly have little tendency to expand their volume of seismicity in the second half of the sequence, in contrast to many of the swarm-like sequences. Symbols are defined as in Figure 6.

like sequences tend to spread slightly, growing by 0 to 50% from the first to the second half of their sequences. In contrast, about half of the remaining sequences grow more, and the swarm-like sequences grow the most and the most consistently. In detail, there is a tendency, even excluding the aftershock-like sequences, for greater growth in cases when the largest event is later in the sequence, but the majority of cases with a distance ratio above 2 in Figure 10 have their largest event before the median time. There is perhaps a tendency for the greatest expansion to strike clusters with the largest event near the median time, but its significance is not clear.

[36] The first-order morphology of seismicity clouds can be analyzed by standard principle value analysis. We compute the autocorrelation matrix summed over all the demeaned hypocentral coordinates of the events in each cluster. The three eigenvalues and corresponding eigenvectors of the matrix define the principle axes and their relative amplitudes. This technique has been applied to many geophysical problems [e.g., *Kirschvink*, 1980; *Vidale*, 1986; *Michelini and Bolt*, 1986; *Shearer et al.*, 2003].

[37] The eigenvector $U_1$, corresponding to the largest eigenvalue $\lambda 1$, gives the axis of minimum rotational inertia, and defines the longest axis of an ellipsoid fit to the hypocenters, while $U_3$, corresponding to the smallest eigenvalue $\lambda 3$, defines the shortest axis of the ellipsoid [*Shearer et al.*, 2003]. The shape of the seismicity cluster can be characterized by the relative sizes of the eigenvalues. A nearly spherical distribution of events has $\lambda 1 \approx \lambda 2 \approx \lambda 3$. Points aligned linearly along a line have $\lambda 1 \gg \lambda 2$, $\lambda 3$ with $U_1$ defining the direction of the line. Points flattened into a plane have $\lambda 3 \ll \lambda 1$, $\lambda 2$ with $U_3$ orthogonal to the plane. $U_1$ and $U_3$ correspond to the least squares solutions for the best fitting line and plane, respectively.

[38] As in the work by *Vidale* [1986], we define the planarity of seismicity hypocenters to be $1 - \lambda 3/\lambda 2$. At its extremes, planarity of 1 indicates perfect planar alignment, and planarity of 0 indicates a similar width and depth of the seismicity cloud, whatever the length.

[39] We chose a planarity value of 0.82 for the sequences, shown binned in Figure 11, as best separating the traditional canonical planar-aftershock pattern on a fault from other patterns. Roughly, the sequences with planarity above 0.82 are visually planar. The distribution of planar and nonplanar seismicity clouds does not bear an obvious relation to the underlying geology and faults, as shown in Figure 12.

[40] The best fitting planes to the seismicity bursts have a strong tendency to be nearly vertical, as shown in Figure 13. Uniformly oriented planes would fill a dip distribution proportional to the sine of the dip angle. The constraint of proximity to the free surface on the stress tensor is that strike-slip planes tend to have a dip near 90° (near vertical), normal faults dip near 60° dip, and thrust faults dip near 30° dip. This suggests that it is mainly strike-slip planes hosting the seismicity bursts, probably related to the dominant strike-slip tectonic style across the study area. However the direction of seismicity shift is indistinguishable from isotropic within the best fit plane, and the long axis of the seismicity ellipsoid also appears randomly distributed within the best fit plane.

[41] Figure 14 shows trends that may give new insights into fault mechanics, deserving of more thorough study than we have space to explore here. Figure 14a shows that more steeply dipping seismicity planes are more planar, perhaps because many strike-slip faults in this area have accumulated more slip than thrust and normal faults over their history, or perhaps simply because normal and thrust faults have more complicated fracture geometries than strike-slip faults. Figure 14b examines these features from another perspective, showing that the least planar faults tend to be strike slip in dominant focal mechanism, many with less steeply dipping planes, although the reason for this is unclear.

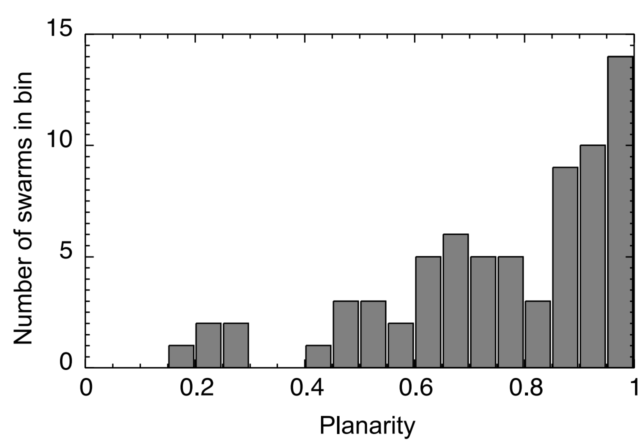


**Figure 11.** Distribution of planarities in the 71 seismicity bursts. A bit less than half show planarity above 0.82, visually quite flat, and this subset is located in Figure 12.

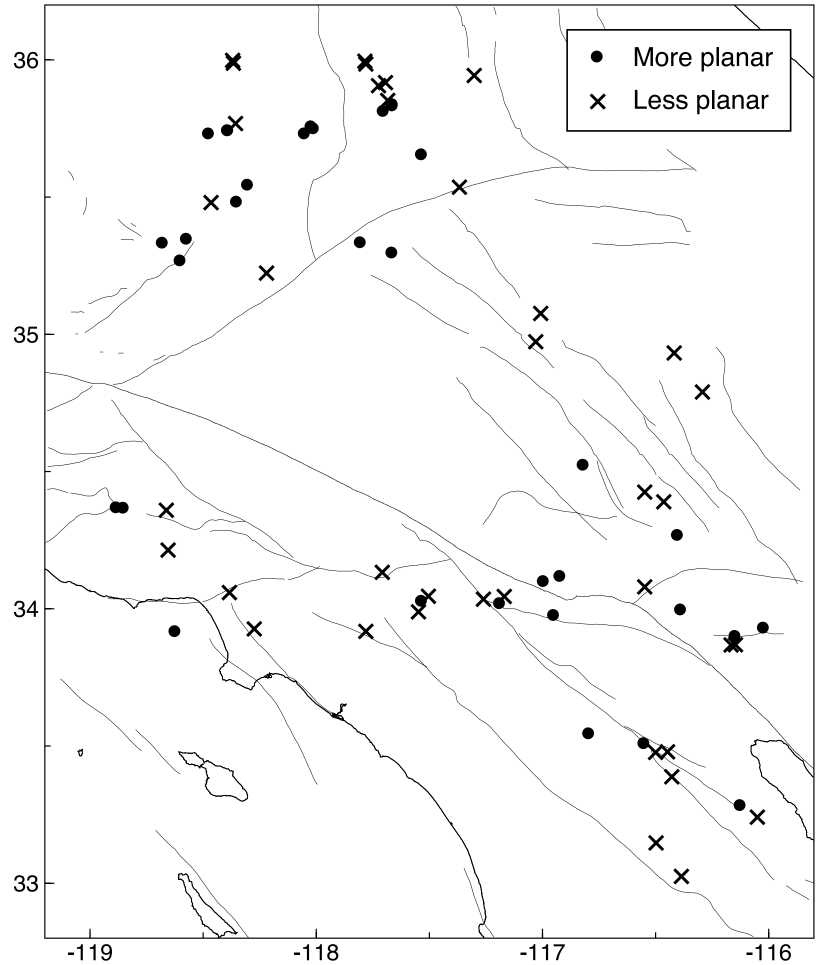


**Figure 12.** Locations of the more and less planar seismicity bursts, as defined by planarity coefficients more than and less than 0.82, respectively.

[42] Swarm-like sequences are most common with normal faulting, there is a mix of swarm-like and aftershock-type mechanisms for strike-slip faulting, and from very little data, thrust faulting shows mostly aftershock-type sequences in Figure 14c.

## 7. Ubiquity of Patterns of Earthquake Cluster Geometry

[43] The seismic sequences range from featureless clouds through lineations and chimneys to sharply defined planes. In general our measurements, although showing some correlations with faulting style, do not establish an association of any particular morphology of seismicity geometry with a particular tectonic province. Figures 1 and 12 give a glimpse of this lack of a pattern, although some consistency of patterns over small areas may be visible. The locations of "swarmy" sequences as indicated by lack of a traditional main shock, compared to those that start with their largest event, are shown in Figure 1. The locations of sequences with high and low planarity are shown in Figure 12.

[44] In summary, the entire study region exhibits a diverse set of burst patterns. The basins of Los Angeles, the main strands of the San Andreas Fault, and the compressive Transverse Ranges all harbor a similar distribution of swarms by our various measures. Nonplanar sequences and "swarmy" sequences, as indicated by lack of an obvious main shock, also do not concentrate at particular depths.

## 8. What Drives Seismic Bursts?

[45] Considerable literature discusses how earthquakes can be triggered by a wide range of geophysical phenomenon, including volcanic eruptions and dike injections, fluid injection [*Ake et al.*, 2005], reservoir loading, tides [*Cochran et al.*, 2004; *Tolstoy and Vernon*, 2002], and, of course, prior earthquakes. In particular, temporal evolution of seismicity patterns and a buildup of seismic activity before the largest event in a swarm sequence have been associated with volcano-tectonic events [e.g., *Jones and Malone*, 2005]. We aim this study at seismicity around tectonic faults, namely, at a major plate boundary, the San Andreas Fault Zone. This study is the first to compare a large number of bursts by applying a variety of different measures, except for a survey solely of swarms around volcanoes [*Benoit and McNutt*, 1996], which in turn had to rely on less uniform and quantitative measures.

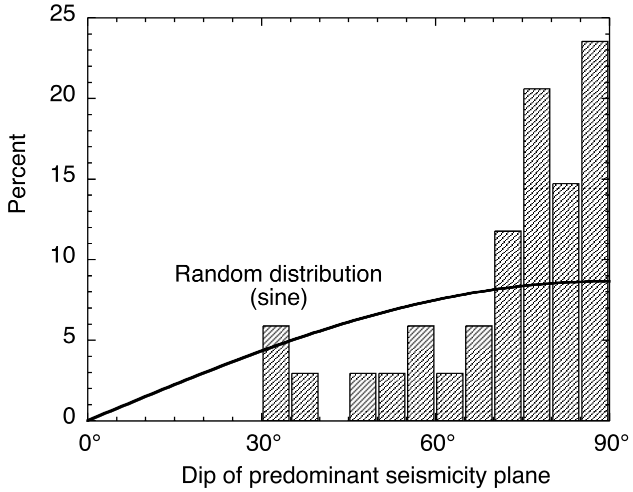


**Figure 13.** Distribution of seismicity plane dip angles in the 34 seismicity bursts with planarity above 0.82. Bursts that are most planar and shallow are particularly concentrated at steep dips. A uniform distribution of fault-normal vectors would have a density of dip angles following the sine of the dip angle. No significant difference is seen in the seismicity plane dip angle between the sequences starting with their largest events and the rest of the sequences. The less planar sequences also show a tendency for steep dips but less strongly, and we have less confidence in the dip measurement.

[46] Three mechanisms are most likely for triggering events to cluster in space and time as observed in swarms. It should be recognized that the triggering mechanism is not necessarily related to the process that loads the faults, which may simply be the long-term tectonic stress accumulation. First, direct triggering from previous earthquakes is the usual explanation of aftershocks. Stress loading can explain many observed features [e.g., *Stein*, 1999], while shaking must be invoked to account for more distant triggering [e.g., *Hill et al.*, 1993]. Cascade models have been extended so that every earthquake has a probability of generating more earthquakes in ETAS models [*Sornette and Sornette*, 1999], which can replicate a wide range of properties in earthquake catalogs.

[47] Second, some bursts of seismicity have been convincingly tied to a rise in fluid pressure at seismogenic depths [*Ake et al.*, 2005; *Raleigh et al.*, 1976]. Other studies argue that strong shaking can redistribute fluid pressure in a way the might trigger earthquakes [*Montgomery and Manga*, 2003]. Still other studies show that the spread of seismicity can obey a diffusion equation, as would perturbations in fluid pressure [*Prejean*, 2002].

[48] Third, aseismic slip can stress faults to failure. "Slow" and "silent" earthquakes have been accompanied by small seismic earthquakes in central California [*Linde et al.*, 1996], episodic acceleration of fault loading correlates with earthquakes [*Nadeau and McEvilly*, 2004], and aseismic fault slip on subduction zones has been suggested to link with earthquakes. In a recent striking observation, a burst near Las Vegas coincided with a GPS-detected strain episode inferred to be caused by dike injection [*Smith et al.*, 2004]. In more complicated models, fluids and aseismic slip have been suggested to work in concert [*Hainzl*, 2004; *Waite and Smith*, 2002].

[49] We can confidently reject the first scenario for many of the bursts. The interval with steady rate of seismicity in

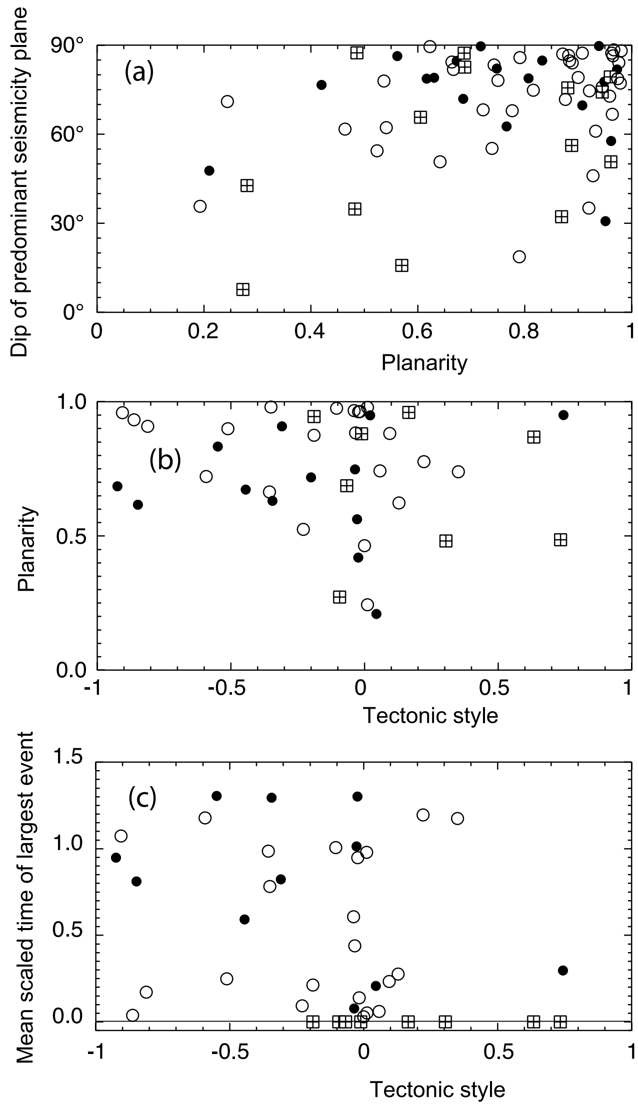


**Figure 14.** Several geometrical observations. (a) Comparison of seismicity plane dip angles with planarity. More vertical planes are more planar, and less steeply dipping planes tend to be aftershock-like. (b) A comparison of seismicity plane flatness and the tectonic style inferred from focal mechanisms. Here −1 is normal faulting, 0 is strike slip, and 1 is reverse faulting. Although such highly nonplanar seismicity geometries are unusual, most with planarity below 0.5 are strike slip. Also, it is apparent that the aftershock-type seismicity bursts tend to occur with strike-slip and thrust, not normal mechanisms. Only 43 of the sequences have some focal mechanisms determined (J. L. Hardebeck, personal communication, 2005). (c) A comparison of the delay of the largest event and the tectonic style. Again −1 is normal faulting, 0 is strike-slip, and 1 is reverse faulting. All the swarm-like sequences with their largest events later than 0.5 scaled time have a negative tectonic style. Symbols are the same as for Figure 6.

Figure 9, the similar number of events over a range of maximum burst magnitudes in Figure 7, the large areas involved in many of the bursts compared to the magnitude of the largest events in the bursts in Figure 6, and the common expansion of the seismicity in Figure 10, all argue that more is involved than just a cascade of earthquakes triggering additional events.

[50] There are arguments for and against both fluid pressure variations and aseismic slip as the driver for our bursts, and a combination of the two is possible [e.g., *Hainzl*, 2004]. The strong expansion of bursts could naturally be explained by fluid diffusion through fractured fault systems, and contrasts with some models of how aseismic slip might proceed. On the other hand, the steady production of seismicity through much of the bursts' most active periods may be consistent with an aseismic slip episode, whereas fluid perturbations might be expected to result in a burst of seismicity more uniformly and rapidly diminishing over time.

[51] Resolution of the cause or causes of bursts might come through focused geodetic monitoring of swarm areas, as in the exciting report of *Smith et al.* [2004] or possibly through repeated monitoring of scattering by repeating earthquakes, if changes due to fluid redistribution are measurable [*Niu et al.*, 2003].

[52] For now, we conclude that swarm-like sequences mark the site of an underlying geophysical disturbance, one of particular interest because it changes the local risk of large earthquakes more than suggested by naive application of Omori's aftershock law [*McGuire et al.*, 2005], but whether that change is large or small remains unresolved.

[53] **Acknowledgment.** This text has benefited from suggestions from Heidi Houston, Jim Dieterich, Greg Beroza, Sebastian Hainzl, Tomas Fischer, Karen Feltzer, Emily Brodsky, and a zealous anonymous reviewer.

## References

Ake, J., K. Mahrer, D. O'Connell, and L. Block (2005), Deep-injection and closely monitored induced seismicity at Paradox Valley, Colorado, *Bull. Seismol. Soc. Am.*, *95*, 664–683.

Astiz, L., and P. M. Shearer (2000), Earthquake locations in the inner Continental Borderland, offshore southern California, *Bull. Seismol. Soc. Am.*, *90*(2), 425–449.

Astiz, L., P. M. Shearer, and D. C. Agnew (2000), Precise relocations and stress change calculations for the upland earthquake sequence in southern California, *J. Geophys. Res.*, *105*(B2), 2937–2953.

Benoit, J. P., and S. R. McNutt (1996), Global volcanic earthquake swarm database 1979–1989, *U.S. Geol. Surv. Open File Rep. 96-69*, 333 pp.

Bird, P., and Y. Y. Kagan (2004), Plate-tectonic analysis of shallow seismicity: Apparent boundary width, beta, corner magnitude, coupled lithosphere thickness, and coupling in seven tectonic settings, *Bull. Seismol. Soc. Am.*, *94*(6), 2380–2399.

Boettcher, M. S., and T. H. Jordan (2004), Earthquake scaling relations for mid-ocean ridge transform faults, *J. Geophys. Res.*, *109*, B12302, doi:10.1029/2004JB003110.

Bräuer, K., H. Kämpf, G. Strauch, and S. M. Weise (2003), Isotopic evidence ($^3He/^4He$, $^{13}C_{CO2}$) of fluid-triggered intraplate seismicity, *J. Geophys. Res.*, *108*(B2), 2070, doi:10.1029/2002JB002077.

Cochran, E., J. E. Vidale, and S. Tanaka (2004), Extreme Earth tides strongly trigger large earthquakes, *Science*, *306*, 1164–1166.

Dreger, D. S., H. Tkalcic, and M. Johnston (2000), Dilational processes accompanying earthquakes in the Long Valley Caldera, *Science*, *288*, 122–125.

Dzurisin, D. (2003), A comprehensive approach to monitoring volcano deformation as a window on the eruption cycle, *Rev. Geophys.*, *41*(1), 1001, doi:10.1029/2001RG000107.

Fischer, T., and J. Horálek (2005), Slip-generated patterns of swarm microearthquakes from West Bohemia/Vogtland (central Europe): Evidence of their triggering mechanism?, *J. Geophys. Res.*, *110*, B05S21, doi:10.1029/2004JB003363.

Hainzl, S. (2004), Seismicity patterns of earthquake swarms due to fluid intrusion and stress triggering, *Geophys. J. Int.*, *159*(3), 1090–1096.

Hainzl, S., and T. Fischer (2002), Indications for a successively triggered rupture growth underlying the 2000 earthquake swarm in Vogtland/NW Bohemia, *J. Geophys. Res.*, *107*(B12), 2338, doi:10.1029/2002JB001865.

Hainzl, S., and Y. Ogata (2005), Detecting fluid signals in seismicity data through statistical earthquake modeling, *J. Geophys. Res.*, *110*, B05S07, doi:10.1029/2004JB003247.

Hainzl, S., G. Zöller, and F. Scherbaum (2003), Earthquake clusters resulting from delayed rupture propagation in finite fault segments, *J. Geophys. Res.*, *108*(B1), 2013, doi:10.1029/2001JB000610.

Henry, C., and S. Das (2001), Aftershock zones of large shallow earthquakes: Fault dimensions, aftershock area expansion and scaling relations, *Geophys. J. Int.*, *147*(2), 272–293.

Hill, D. P., W. L. Ellsworth, M. J. S. Johnston, J. O. Langbein, D. H. Oppenheimer, A. M. Pitt, P. A. Reasenberg, M. L. Sorey, and S. R. McNutt (1990), The 1989 earthquake swarm beneath Mammoth Mountain, California: An initial look at the 4 May through 30 September activity, *Bull. Seismol. Soc. Am.*, *80*(2), 325–339.

Hill, D. P., et al. (1993), Seismicity remotely triggered by the magnitude 7.3 Landers, California, earthquake, *Science*, *260*, 1617–1623.

Horálek, J., J. Sileny, and T. Fischer (2002), Moment tensors of the January 1997 earthquake swarm in NW Bohemia (Czech Republic): Double-couple vs. non-double-couple events, *Tectonophysics*, *356*(1–3), 65–85.

Hough, S. E., R. S. Dollar, and P. Johnson (2000), The 1998 earthquake sequence south of Long Valley Caldera, California: Hints of magmatic involvement, *Bull. Seismol. Soc. Am.*, *90*(3), 752–763.

Jones, J., and S. D. Malone (2005), Mount Hood earthquake activity: Volcanic or tectonic origins?, *Bull. Seismol. Soc. Am.*, *95*(3), 818–832.

Jones, L. M., and P. Molnar (1979), Some characteristics of foreshocks and their possible relationship to earthquake prediction and premonitory slip on faults, *J. Geophys. Res.*, *84*, 3596–3608.

Kanamori, H. (1977), The energy release in great earthquakes, *J. Geophys. Res.*, *82*, 2981–2987.

Kirschvink, J. L. (1980), The least-squares line and plane and the analysis of palaeomagnetic data, *Geophys. J. R. Astron. Soc.*, *62*, 699–718.

Lay, T., and T. C. Wallace (1995), *Modern Global Seismology*, xii, 521 pp., Elsevier, New York.

Linde, A. T., M. T. Gladwin, M. J. S. Johnston, R. L. Gwyther, and R. G. Bilham (1996), A slow earthquake sequence on the San Andreas fault, *Nature*, *383*, 65–68.

Magistrale, H. (2002), Relative contributions of crustal temperature and composition to controlling the depth of earthquakes in southern California, *Geophys. Res. Lett.*, *29*(10), 1447, doi:10.1029/2001GL014375.

McGuire, J. J., M. S. Boettcher, and T. H. Jordan (2005), Foreshock sequences and short-term earthquake predictability on East Pacific Rise transform faults, *Nature*, *434*(7032), 457–461.

Michelini, A., and B. A. Bolt (1986), Application of the principal parameter method to the 1983 Coalinga, California, aftershock sequence, *Bull. Seismol. Soc. Am.*, *76*, 409–420.

Mogi, K. (1963), Some discussions on aftershocks, foreshocks, and earthquake swarms: The fracture of a semi-infinite body caused by an inner stress origin and its relation to the earthquake phenomenon, *Bull. Earthquake Res. Inst. Univ. Tokyo*, *41*, 615–658.

Montgomery, D. R., and M. Manga (2003), Streamflow and water well responses to earthquakes, *Science*, *300*, 2047–2049.

Nadeau, R. M., and T. V. McEvilly (2004), Periodic pulsing of characteristic microearthquakes on the San Andreas Fault, *Science*, *303*, 220–222.

Niu, F. L., P. G. Silver, R. M. Nadeau, and T. V. McEvilly (2003), Migration of seismic scatterers associated with the 1993 Parkfield aseismic transient event, *Nature*, *426*(6966), 544–548.

Omori, F. (1895), On the aftershocks of earthquakes, *J. Coll. Sci. Imp. Univ. Tokyo*, *7*, 111–200.

Prejean, S. G. (2002), The interaction of tectonic and magmatic processes in the Long Valley caldera, California, Ph.D. thesis, Stanford Univ., Palo Alto, Calif.

Prejean, S., A. Stork, W. Ellsworth, D. Hill, and B. Julian (2003), High precision earthquake locations reveal seismogenic structure beneath Mammoth Mountain, California, *Geophys. Res. Lett.*, *30*(24), 2247, doi:10.1029/2003GL018334.

Raleigh, C. B., J. H. Healy, and J. D. Bredehoeft (1976), An experiment in earthquake control at Rangeley, Colorado, *Science*, *191*, 1230–1237.

Scholz, C. H. (1990), *The Mechanics of Earthquakes and Faulting*, 439 pp., Cambridge Univ. Press, New York.

Shearer, P. M. (1997), Improving local earthquake locations using the L1 norm and waveform cross correlation: Application to the Whittier Narrows, California, aftershock sequence, *J. Geophys. Res.*, *102*, 8269–8283.

Shearer, P. M. (1998), Evidence from a cluster of small earthquakes for a fault at 18 km depth beneath Oak Ridge, southern California, *Bull. Seismol. Soc. Am.*, *88*, 1327–1336.
Shearer, P. M. (2002), Parallel fault strands at 9-km depth resolved on the Imperial Fault, southern California, *Geophys. Res. Lett.*, *29*(14), 1674, doi:10.1029/2002GL015302.
Shearer, P. M., J. L. Hardebeck, L. Astiz, and K. B. Richards-Dinger (2003), Analysis of similar event clusters in aftershocks of the 1994 Northridge, California, earthquake, *J. Geophys. Res.*, *108*(B1), 2035, doi:10.1029/2001JB000685.
Shearer, P. M., E. Hauksson, and G. Lin (2005), Southern California hypocenter relocation with waveform cross-correlation: Part 2. Results using source-specific station terms and cluster analysis, *Bull. Seismol. Soc. Am.*, *95*(3), 904–915, doi:10.1785/0120040168.
Shearer, P. M., G. Prieto, and E. Hauksson (2006), Comprehensive analysis of earthquake source spectra in southern California, *J. Geophys. Res.*, doi:10.1029/2005JB003979, in press.
Smith, K. D., D. von Seggern, G. Blewitt, L. Preston, J. G. Anderson, B. P. Wernicke, and J. L. Davis (2004), Evidence for deep magma injection beneath Lake Tahoe, Nevada-California, *Science*, *305*, 1277–1280.
Sornette, A., and D. Sornette (1999), Renormalization of earthquake aftershocks, *Geophys. Res. Lett.*, *26*, 1981–1984.
Stein, R. S. (1999), The role of stress transfer in earthquake occurrence, *Nature*, *402*, 605–609.
Tajima, F., and H. Kanamori (1985a), Aftershock area expansion and mechanical heterogeneity of fault zone within subduction zones, *Geophys. Res. Lett.*, *12*, 345–348.
Tajima, F., and H. Kanamori (1985b), Global survey of aftershock area expansion patterns, *Phys. Earth Planet. Inter.*, *40*(2), 77–134.
Tolstoy, M., and F. Vernon (2002), Breathing of the seafloor: Tidal correlations of seismicity at Axial volcano, *Geology*, *30*, 503–506.
Vidale, J. E. (1986), Complex polarization analysis of particle motion, *Bull. Seismol. Soc. Am.*, *76*, 1393–1405.
Waite, G. P., and R. B. Smith (2002), Seismic evidence for fluid migration accompanying subsidence of the Yellowstone caldera, *J. Geophys. Res.*, *107*(B9), 2177, doi:10.1029/2001JB000586.

P. M. Shearer, SIO-IGPP, University of California, San Diego, La Jolla, CA 92093-0225, USA. (pshearer@ucsd.edu)
J. E. Vidale, IGPP, University of California, Los Angeles, CA 90095-1567, USA. (vidale@ucla.edu)